Ultrasound Concave 2D Ring Array for Retinal Stimulation

SUBMISSION DATE / POSTED DATE

23-03-2023 / 27-03-2023

CITATION

Lu, Jian-yu; Lu, Gengxi; Thomas, Biju; Humayun, Mark; Zhou, Qifa (2023): Ultrasound Concave 2D Ring Array for Retinal Stimulation. TechRxiv. Preprint. https://doi.org/10.36227/techrxiv.22323127.v1

DOI

10.36227/techrxiv.22323127.v1

Ultrasound Concave 2D Ring Array for Retinal Stimulation

Jian-yu Lu, *Fellow*, *IEEE*, Gengxi Lu, Biju Thomas, Mark Humayun, *Fellow*, *IEEE*, and Qifa Zhou, *Fellow*, *IEEE*

***Abstract*— An ultrasound concave 2D ring array transducer was designed for visual stimulation of the retina to restore vision in blind people. The array has a frequency of 20 MHz (0.075-mm wavelengths in water), 18-mm focal length (the curvature of the concave array), 1004 elements (with a pitch of 4.0 wavelengths), and inner and outer diameters of 9 mm and 14 mm respectively. Images produced with the array at the focal distance were simulated with a computer. Results show that the images obtained can achieve a full-width-at-half-maximum (FWHM) resolution of 0.147 mm that is very close to the FWHM diffraction limit (0.136 mm). In addition, a scaled experiment at a lower frequency of 2.5 MHz was performed. The result is very close to those obtained with the simulations.**

***Index Terms*— Concave 2D ring array transducer; Ultrasound; Stimulation of retina cells; Visual stimulation of the brain; High-frequency ultrasound; and Limited-diffraction beams.**

[1]

I. Introduction

Many people suffer from eye diseases such as age-related macular degeneration (AMD) [1] and retinitis pigmentosa (RP) [2], which lead to blindness. Efforts of vision restoration for blind people have been studied for many years [3-6]. The methods used include direct stimulation of the visual cortex of the brain [3], or implanting a chemical biomimetic chip [4] or an array of electrodes [5-6] on retina to stimulate the retina cells that subsequently stimulate the corresponding neurons in the brain. For electrode array stimulation of the retina, optical images are converted into electrical signals and projected onto the electrode array. The electrical images are then mapped to the corresponding neurons in the brain to obtain visual perception. Retinal prostheses such as Argus II which is based on this principle are now commercially available [7]. Although the implant-based techniques are successful to restore vision, they are invasive since surgical procedures are needed to insert the chemical biomimetic chip or electrode array into the retina. The surgical procedures may cause medical complications and take time to recover. Also, there may be adverse reactions between the eye tissues and the implants.

To overcome the invasive nature and associated medical complications of the surgical procedure to implanted devices such as biomimetic chip and electrode array, efforts have been made over many years to use ultrasound as an alternative method to stimulate the cells in the retina to restore vision non-invasively [8-14]. Recently, focused ultrasound has been used to stimulate the cells in the retina *in vivo* and these cells subsequently stimulate the corresponding neurons in the brain of a rat [12-13]. When the focused ultrasound stimuli were moved across the retina in a specific pattern, a corresponding change in the pattern of the neuronal activities (electrical signals) were recorded by the electrode array placed on the visual cortex [12-13]. Although the study is useful to demonstrate that ultrasound can be used to stimulate the retina that subsequently stimulates the brain, it does not stimulate multiple spots on the retina simultaneously. Also, the stimulation effect is slow and hence may not produce a natural vision of an entire object.

To produce a vision perception that is similar to viewing optical images of moving objects for blind people, it is desirable to produce real-time and dynamic ultrasound patterns on the retina to stimulate multiple spots simultaneously, instead of the point-by-point stimulation [10, 15-16]. In this paper, we designed a high-frequency concave two-dimensional (2D) ultrasound ring array transducer used as a prosthesis that can be mounted on the surface of an eyeball to stimulate the cells on the retina for vision restoration [17]. The advantage of using a ring array transducer is to avoid the heavy attenuation of ultrasound by the lens of the eye, especial at a high ultrasound frequency, and avoid the heating of the lens. The concave shape of the ring array transducer allows better fitting of the array with the shape of the eyeball. By selecting the proper curvature of the array transducer, ultrasound can be focused on the retina to produce real-time images. Also, the concave shape of the 2D ring array transducer allows a smaller number of elements to be used for the array transducer to produce images on the retina since the phase shifts needed to focus ultrasound beams are obtained through the concave shape of the array. This reduces the number of electrical connections to the array, and thereby simplified the driving circuits and the imaging system. Using a high-frequency ultrasound (20 MHz), the size of the array transducer can be made small enough to fit on the eyeball and a higher image resolution can be achieved.

This work was supported in part by the grants R01EY026091, R01EY028662, R01EY030126 and P30EY029220 from the National Institutes of Health (NIH), and an unrestricted departmental grant from research to prevent blindness.

Jian-yu Lu is with the Department of Bioengineering, The University of Toledo, Toledo, Ohio 43606, USA. (e-mail: jian-yu.lu@ieee.org).

Gengxi Lu, Biju Thomas, Mark Humayun, and Qifa Zhou are all with the USC Ginsburg Institute for Biomedical Therapeutics, University of Southern California, Los Angeles, CA 90033, the Roski Eye Institute, Department of Ophthalmology, University of Southern California, Los Angeles, CA 90033, USA, and the Department of Biomedical Engineering University of Southern California, Los Angeles, California 90007, USA

This paper is organized as follows. A brief theory for the concave ultrasound ring array transducer will be presented in Section II. Then, computer simulations and a scaled experiment will be given in Section III. The results of the simulations and the experiment will be shown in Section IV. Finally, discussion and conclusion will be given in Sections V and VI respectively.

II. Theoretical Preliminaries

A brief theoretical description of the method is given below [18]. The isotropic/homogeneous wave equation is given by [19]:

$$\left[\nabla^2 - \frac{1}{c^2}\frac{\partial^2}{\partial t^2}\right]\Phi(\vec{r},t) = 0, \tag{1}$$

where $\nabla^2 = \partial^2/\partial x^2 + \partial^2/\partial y^2 + \partial^2/\partial z^2$ is the Laplacian, $\Phi(\vec{r},t)$ is acoustic pressure, velocity potential, or Hertz potential in free space, $\vec{r} = (x, y, z)$ is a point in the space, t is the time, c is the speed of sound of the medium or the speed of light in vacuum. Using Fourier transform relationship, a solution to the wave equation can be expressed as:

$$\Phi(\vec{r}_0,t) = \frac{1}{2\pi}\int_{-\infty}^{\infty}\tilde{\Phi}(\vec{r}_0;\omega)e^{-i\omega t}d\omega, \tag{2}$$

where $\tilde{\Phi}(\vec{r}_0;\omega)$ is the Fourier transform of $\Phi(\vec{r}_0,t)$ in terms of time, $\vec{r}_0 = (x_0, y_0, z)$ is a spatial point where ultrasound field is produced, $\omega = 2\pi f$ is the angular frequency, and f is the frequency.

It is easy to verify that the following limited-diffraction array beam [20-23] $\Phi^{uv}_{Array}(\vec{r}_0,t)$ is a solution to the wave equation in Eq. (1):

$$\begin{aligned}\Phi^{uv}_{Array}(\vec{r}_0,t) &= \frac{1}{2\pi}\int_0^{\infty}A(k)D_{u,v}(\omega)e^{ik_{x_u}x}e^{ik_{y_v}y}e^{ik_{z_{uv}}z}e^{-i\omega t}dk \\ &= \frac{1}{2\pi}\int_{-\infty}^{\infty}A(k)H(k)D_{u,v}(\omega)e^{i\vec{k}_{uv}\cdot\vec{r}-i\omega t}dk\end{aligned}, \tag{3}$$

where the subscript "Array" means array beam, u and v are integers, $k = \omega/c$ is the wave number, $A(k)$ is the electro-mechanical transfer function of a transducer, $D_{u,v}(\omega)$ are complex coefficients, $H(k)$ is the Heaviside step function $H(\frac{\omega}{c}) = \begin{cases}1, & \omega \ge 0\\ 0, & \omega < 0\end{cases}$ [24], $\vec{k}_{uv} = (k_{x_u}, k_{y_v}, k_{z_{uv}})$ is the wave vector, where k_{x_u} and k_{y_v} are the x and y components of the wave vector respectively, and $k_{z_{uv}} = \sqrt{k^2 - k_{x_u}^2 - k_{y_v}^2}$ with $k^2 \le k_{x_u}^2 + k_{y_v}^2$ for propagating waves and $k_{x_u}^2 + k_{y_v}^2 > k^2$ for evanescent waves. From Eq. (3), one obtains the spectrum of $\Phi^{uv}_{Array}(\vec{r}_0,t)$ as follows:

$$\tilde{\Phi}^{uv}_{Array}(\vec{r}_0;\omega) = \frac{A(k)H(k)}{c}D_{u,v}(\omega)e^{i\vec{k}_{uv}\cdot\vec{r}}. \tag{4}$$

Assuming that the system is linear, the total field at $\vec{r}_0$ is a linear superposition of those produced by Eq. (4) (assuming that the summation exists):

$$\tilde{\Phi}(\vec{r}_0;\omega) = \sum_{u=-\infty}^{\infty}\sum_{v=-\infty}^{\infty}\frac{A(k)H(k)}{c}D_{u,v}(\omega)e^{i\vec{k}_{uv}\cdot\vec{r}}. \tag{5}$$

Now, let's determine the coefficients, $D_{u,v}(\omega)$, for a 2D array of a given aperture weighting function. Assuming that a planar 2D array transducer is located at the plane $z = 0$ and the field produced at the transducer surface is given by:

$$\tilde{\Phi}_1(\vec{r}_1;\omega) = \begin{cases}\tilde{Q}(\vec{r}_1;\omega), & (|x_1| \le w_x,\ |y_1| \le w_y)\\ 0, & (w_x < |x_1| \le R_x,\ w_y < |y_1| \le R_y)\end{cases}, \tag{6}$$

where $\tilde{Q}(\vec{r}_1;\omega)$ is the field at the surface of the transducer, $\vec{r}_1 = (x_1, y_1, 0)$ is a point at the surface, w_x and w_y are the half widths of the aperture size of the array transducer along the x_1 and y_1 axes, respectively. The array transducer is assumed to be surrounded by a rectangular frame $(w_x < |x_1| \le R_x,\ w_y < |y_1| \le R_y)$ with zero field amplitude, where R_x and R_y are the half widths of the outer frame. In addition, the aperture weighting pattern in Eq. (6) is periodically repeated outside of the frame bounded by $(|x_1| \le R_x,\ |y_1| \le R_y)$ with periods of $2R_x$ and $2R_y$ in the x_1 and y_1 directions, respectively. Apparently, as both $R_x \to \infty$ and $R_y \to \infty$, Eq. (6) represents a single array without a spatial repetition.

Since Eq. (6) is a periodic function, it can be expanded as a Fourier series [24] with periods of $2R_x$ and $2R_y$ along the x_1 and y_1 axes, respectively. Letting $z = 0$ in Eq. (5), we obtain such a series:

$$\tilde{\Phi}_1(\vec{r}_1;\omega) = \sum_{u=-\infty}^{\infty}\sum_{v=-\infty}^{\infty}\frac{A(k)H(k)}{c}D_{u,v}(\omega)e^{ik_{x_u}x_1}e^{ik_{y_v}y_1}, \tag{7}$$

where $k_{x_u} = u\pi/R_x$ and $k_{y_v} = v\pi/R_y$, and $u, v = \pm 1, \pm 2, \pm 3, \cdots$. The coefficients of the Fourier series in Eq. (7) are given by [24]:

$$\begin{aligned}&\frac{A(k)H(k)}{c}D_{u,v}(\omega) \\ &= \frac{1}{4R_xR_y}\int_{-w_x}^{w_x}\int_{-w_y}^{w_y}\tilde{\Phi}_1(\vec{r}_1;\omega)e^{-ik_{x_u}x_1}e^{-ik_{y_v}y_1}dx_1dy_1\end{aligned}. \tag{8}$$

Assuming that an array transducer consists of $M \times N$ rectangular elements and the spatially quantized driving or aperture weighting function of an element centered at (x_{1_m}, y_{1_n}) is $\tilde{\Phi}_{1_{m,n}}(\omega) = \tilde{\Phi}_1(x_{1_m}, y_{1_n};\omega)$, where $1 \le m \le M$, $1 \le n \le N$,

and M and N are integers, Eq. (8) can be pre-calculated and stored as known coefficients as follows:

$$\frac{A(k)H(k)}{c}D_{u,v}(\omega)=\frac{1}{R_xR_y}\sum_{m=1}^{M}\sum_{n=1}^{N}w_{x_m}w_{y_n}\tilde{\Phi}_{1_{m,n}}(\omega)\,\mathrm{sinc}(k_{x_u}w_{x_m})\,\mathrm{sinc}(k_{y_v}w_{y_n})e^{-ik_{x_u}x_{1_m}-ik_{y_v}y_{1_n}}, \quad (9)$$

where w_{x_m} and w_{y_n} are the half widths of the transducer element centered at (x_{1_m}, y_{1_n}) along the x_1 and y_1 axes, respectively, and sinc(·) is the sinc function. Using Eq. (9), the 2D Fourier series in Eq. (5) can be evaluated with an inverse fast Fourier transform or IFFT [25].

Notice that the aperture weighting function $\tilde{\Phi}_1(\vec{r}_1;\omega)$ in Eq. (8) can be approximately written as:

$$\tilde{\Phi}_1(\vec{r}_1;\omega)\approx\tilde{\Phi}'_1(\vec{r}_1;\omega)\exp\{-i[k/(2F)](x_1^2+y_1^2)\}, \quad (10)$$

where $\tilde{\Phi}'_1(\vec{r}_1;\omega)$ is the aperture weighting function without the focusing term $\exp\{-i[k/(2F)](x_1^2+y_1^2)\}=\exp\{-i[k/(2F)]r_1^2\}$ that is due to the curvature of the spherically-curved concave ring array transducer with a focal distance $z=F$, where F is the focal length and $r_1=\sqrt{x_1^2+y_1^2}$. According to Goodman [26], $\tilde{\Phi}_1(\vec{r}_1;\omega)$ is approximately related to the ultrasound image $\tilde{\Phi}(x_0,y_0,z=F;\omega)$ at the focal distance F (at the retina of the eyes) of the transducer through the Fresnel diffraction integral, or, $\tilde{\Phi}'_1(\vec{r}_1;\omega)$ can be written as the following spatial 2D Fourier transform $\mathfrak{F}_{x_1,y_1}\{\cdot\}$ in terms of x_1 and y_1 (see Eq. (28) of [27]):

$$\tilde{\Phi}(x_0,y_0,z=F;\omega)=\frac{e^{ikF}}{i\lambda F}(1+\frac{i\lambda}{2\pi F})e^{i\frac{k}{2F}(x_0^2+y_0^2)}\mathfrak{F}_{x_1,y_1}\{\tilde{\Phi}'_1(\vec{r}_1;\omega)\}(k_{x_0},k_{y_0}), \quad (11)$$

where λ is the wavelength, $k_{x_0}=kx_0/F$, and $k_{y_0}=ky_0/F$. If the wave source has a dimension $D\times D$, the integration limits of the Fourier transform will be from $-a$ to a, where $D=2a$.

Assuming that the optical image formed at the retina of the eyes of blind people can be approximated with an ultrasound image $\tilde{\Phi}(x_0,y_0,z=F;\omega)$ that is used for a visual stimulation of the brain, the driving function of the concave 2D ring array transducer can be calculated by the inverse Fourier transform of Eq. (11) as follows (see Eq. (38) of [27]):

$$\tilde{\Phi}'_1(\vec{r}_1;\omega)=[i\lambda Fe^{-ikF}(1+\frac{i\lambda}{2\pi F})^{-1}]\int_{-\infty}^{\infty}\int_{-\infty}^{\infty}[\tilde{\Phi}(x_0,y_0,z=F;\omega)e^{-i\frac{k}{2F}(x_0^2+y_0^2)}]e^{i(k_{x_0}x_1+k_{y_0}y_1)}dk_{x_0}dk_{y_0}. \quad (12)$$

If the images are formed on a spherical surface such as the retina with a radius of curvature of F, the phase term $\exp[-i[k/(2F)](x_0^2+y_0^2)]=\exp(-i[k/(2F)]r_0^2)$ in Eq. (12) should be removed when doing the inverse Fourier transform.

After getting $\tilde{\Phi}'_1(\vec{r}_1;\omega)$ from Eq. (12), one can get $\tilde{\Phi}_1(\vec{r}_1;\omega)$ using Eq. (10). Inserting $\tilde{\Phi}_1(\vec{r}_1;\omega)$ into Eq. (8) and using Eq. (9), one obtains $D_{u,v}(\omega)$. Ultrasound images can then be obtained with Eq. (5) for visual stimulation of the brain of the blind people so that they could "see" the objects (note that usually a long tone burst is needed in ultrasound visual stimulation of the retina and thus $A(k)$ is approximately a delta function with a fixed $k=\omega/c$ or angular frequency ω due to a narrow bandwidth of the driving signal, and thus Eq. (5) instead of Eq. (2) can be used to calculate the ultrasound field).

III. METHOD

A. Computer Simulation

Based on the above theory, an ultrasound concave 2D ring array transducer suitable for the study of larger animals such as rabbits was designed which is capable to produce a high-resolution image on retina for visual stimulation of the brain. The curvature of the array is the same as the focal length of the array and is given by $F=F_1=18$ mm. The center frequency of the array is $f=f_1=20$ MHz. The inner diameter (I.D.) of the array is set to 0, 6, and 9 mm to investigate how image quality is affected by these changes, and the outer diameter (O.D.) of the array is $D=D_1=14$ mm. Assuming that the medium where the ultrasound propagates is similar to water that has a speed of sound of about $c=1500$ m/s, the wavelength of the ultrasound is $\lambda=\lambda_1=0.075$ mm. A summary of the parameters of the concave 2D ring array transducer is given in Table 1.

To evaluate the performance of the array, computer simulations were conducted. In the simulations, a digital phantom that is consists of 30 point objects with a height $h=h_1=2.5$ mm between the top-most and bottom-most rows of point objects was assumed (see the "Desired Pattern" on the upper-left corner of Fig. 1). For normal people, an optical image of the digital phantom will be formed on the retina to produce vision. For blind people, the digital phantom has to be converted to an ultrasound image on the retina to stimulate cells that subsequently stimulate the neurons in the brain for vision perception. To produce an ultrasound image on the retina, an inverse spatial Fourier transform [24] of the digital phantom $\tilde{\Phi}(x_0,y_0,z=F;\omega)$ was performed using Eq. (12) to get $\tilde{\Phi}'_1(\vec{r}_1;\omega)$ (implemented with an IFFT [25]) based on the Fresnel approximation [26-27]. Then, ultrasound image on the retina was obtained from Eq. (5) using the relationship in Eqs. (9) and (10) [18,27], where w_{x_m} and w_{y_n} in Eq. (9) were the half width of the pitch (distance between the centers of two adjacent elements) of the concave 2D ring array transducer and were assumed to be equal for all array elements.

TABLE 1. Parameters of the 20-MHz concave 2D ring array transducer.

Parameters	Values
Frequency / Wavelength	20 MHz / 0.075 mm
Outer Diameter (O.D.)	14 mm
Inner Diameter (I.D.)	9 mm
Curvature of Array (Focal Length)	18 mm

B. Experiment

In addition to the simulations, an experiment was performed [28]. In a linear system, the total ultrasound field produced by a 2D array transducer can be viewed as a summation of the field produced by each individual array element. Also, the field of each element is a superposition of the fields produced by point sources within the element and each point source produces a spherical wave. In practice, it is not possible to get a point source. However, if the size of a transducer element is small as compared to the wavelength and the distance from the element is much larger than the size of the element, the field produced by the element will be close to a spherical wave. Combining the fields of such small elements, the field of a larger element of a 2D array transducer can be produced. Thus, an experiment that measures the spherical wave can be performed to produce the field of a concave 2D ring array transducer to obtain images on the retina for visual stimulation of the brain.

In the experiment, the center element of an existing 10-ring and 50-mm diameter Bessel annular array transducer that was used to produce limited-diffraction beams was used to produce a spherical wave [29-31]. The transducer was made of 1-3 ceramic/polymer composite, had a center frequency of $f = f_2$ = 2.5 MHz, and was broadband with its -6dB fractional bandwidth of about 81% of the center frequency. The diameter of the center element of the annual array was about 4 mm. To reduce the size of the center element to produce a good spherical wave, a 1-mm thick foam tape (3M Microfoam, 3M Commercial Office Supply Division, St. Paul, MN) with a 1-mm diameter hole was attached in the front of the center element and aligned with the center of the element [28].

The center element of the transducer was driven by a 1.5-cycle and 2.5-MHz sine-wave pulse, and the acoustic pressure of the pulse was measured at distance z = 100 mm with a 0.5-mm diameter broadband PVDF needle hydrophone (NTR 1000, NTR System, Inc., Seattle, WA) in water [28]. The signal measured was digitized with an 8-bit analog-to-digital (A/D) converter at a sampling rate of 40 MS/s for 300 samples [28]. Since the effective size of the center element was about 1.7 wavelengths at 2.5 MHz (the wavelength was about $\lambda = \lambda_2$ = 0.6 mm at the speed of sound of about c = 1500 m/s in water), in the far field at z = 100 mm, a good approximation of the spherical wave was obtained. The hydrophone was scanned in the direction that was perpendicular to the z axis (i.e., the axis from the point source on the transducer surface towards the starting point of the hydrophone) over a distance of 50 mm (starting from the axis), with a step size of 0.2 mm for 250 steps. At each step, the transducer was excited and 300 samples of the signal mentioned above was acquired and stored on a hard disk. This process was repeated until data were acquired from all steps.

For ultrasound visual stimulation, a long tone burst with many cycles is needed to deliver enough power to the cells on the retina. In this case, the signal has a very narrow bandwidth and it can be approximately viewed as containing a single frequency. To get single-frequency (also called continuous wave or CW) signals, the broadband signals measured from the experiment above were Fourier transformed first and then the 2.5-MHz signals were extracted for all 250 scanning steps. Since the spherical wave is axially symmetric, the ultrasound wave on a plane that is perpendicular to the z axis will be also axially symmetric. Thus, to get the signals on 2D rectangular grids with 0.2-mm pitch over a planar surface of 100-mm diameter, the data from the 250 steps were rotated around the z axis using one-dimensional (1D) interpolations along the radial direction (the rotation angle was continuous).

Because of the reciprocal principle, the pulse field measured above is the same as that when ultrasound is transmitted from each of the positions of the hydrophone across the planar 2D array surface and the signal is measured at the fixed position of the point transmitter. This allows to weight the measured signals in the area between the inner and outer rings of the 2D grids with the function $\tilde{\Phi}_1(\vec{r}_1;\omega)$ obtained from Eqs. (12) and (10) to form an effective 2D ring array transducer to produce an ultrasound image of the object (digital phantom) at the focal distance $F = F_2$ = 100 mm.

Since the low-frequency (2.5 MHz) ring array transducer with 100-mm focal length and $D = D_2$ = 46.67-mm outer diameter was used for the experiment, a proper scaling of the digital phantom is needed so that the result of the experiment is comparable to that obtained with the high-frequency (20 MHz) ring array transducer of a smaller focal length of 18 mm and a smaller outer diameter of 14 mm. Because image resolution (a higher resolution means a smaller beam width) at focus is inversely proportional to the wavelength and the f-number (focal length divided by the diameter of the aperture or the outer diameter of the ring array transducer) (see Eq. (37) of [27]), the scaling factor s of the digital object can be calculated with the following formula:

$$s = \frac{f-\text{number2}}{f-\text{number1}} \times \frac{\lambda_2}{\lambda_1}, \tag{13}$$

where $f-\text{number2} = F_2 / D_2$ = 2.143 and $f-\text{number1} = F_1 / D_1$ = 1.286 are the $f-\text{number}$ of the 2.5-MHz and 20-MHz ring array transducers respectively, and λ_2 = 0.6 mm and λ_1 = 0.075 mm are their respective wavelengths. This gives s = 13.33 and thus the height of the scaled digital phantom is given by $h = h_2 = sh_1$ = 33.33 mm.

Using the scaled digital phantom and taking into consideration of the focal length of F_2 = 100 mm and the diameter of the outer ring D_2 = 46.67 mm, the weighting function of the concave 2D ring array transducer can be obtained from Eq. (12) to produce ultrasound images at the focal distance F_2.

IV. Results

A. Computer Simulation

The results of the computer simulation [18] are given in Fig. 1 where the image dimensions are given in the figure. As mentioned before, the digital phantom that consists of 30 point objects is at the upper-left corner of the figure and is labeled as "Desired Pattern". The phantom is an image that the blind people would see. The height between the top-most and the bottom-most point objects of the digital phantom is 2.5 mm. Figs. 1(a)-1(i) are simulated [18] images of the digital phantom obtained with the 20-MHz concave 2D ring array transducer (see Table 1 except that the inner diameter is varied for comparisons) at its focal distance of 18 mm. Images in the top, middle, and bottom rows of Figs. 1(a)-1(i) were obtained with the 2D ring array transducer of pitches of 1.5 λ_1, 4.0 λ_1, and 5.6 λ_1, corresponding to the number of array elements of N =7131, 1004, and 512 when the inner diameters (I.D.) was 9 mm. From the left to right columns of Figs. 1(a)-1(i), images were obtained with I.D. of 0 mm, 6 mm, and 9 mm, respectively. It is clear from the results that as the number of transducer elements increases, image quality increases. Also, as the inner diameter of the concave 2D array transducer increases, the image quality decreases. At the 5.6 λ_1 pitch, aliasing artifacts due to an inadequate spatial sampling rate of the drive signals can be clearly seen in the images. To exclude the lens of the eye, it is necessary to have a large enough I.D. (9 mm for rabbits) since ultrasound attenuation of the lens is high. Thus, as a compromise, the image in Fig. 1(f) with a pitch of 4.0 λ_1 and an I.D. of 9 mm were used to determine the parameters of the concave 2D ring array transducer (see Table 1).

For quantitative comparison of resolution and sidelobes of the ultrasound images obtained by the 20-MHz concave 2D ring array transducer, line plots of the normalized magnitude of ultrasound pressure through the center of the bottom 5 point objects of the images in Figs. 1(d) (I.D. = 0 mm, solid line), 1(e) (I.D. = 6 mm, dotted line), and 1(f) (I.D. = 9 mm, dashed line) were obtained and shown in Fig. 2. The full-width-at-half-maximum (FWHM) value of the line plot of the center point object when I.D. = 0 mm (Fig. 1(d)) is about 0.147 mm, which is very close to the theoretical value of the FWHM of $0.141\lambda_1 F_1 / D_1$ = 0.136 mm calculated with Eq. (36) of [27]. It is clear from the plots that as the I.D. value increases (more central elements are removed), the sidelobes of the images will also increase, although the resolution is increased slightly with larger inner diameters. Higher sidelobes reduce image contrast and thus lower the image quality.

Fig. 3(a) and 3(b) show the amplitude and phase of the driving function for each element of the concave 2D ring array transducer to produce the image in Fig. 1(f) (pitch = 4.0 λ_1, N = 1004, and I.D. = 9 mm). It is clear that with the concave design of the array transducer, the phase change is relatively smooth across the array surface, which allows a bigger pitch (4.0 λ_1) and thus a smaller number of elements (1004) to be used for getting a reasonably good image. Without the concave design, electronic focusing is required and thus a smaller size of the array elements is needed to avoid spatial aliasing, increasing the number of elements and thus the complexity of the imaging system.

B. Experiment

Fig. 4(a) is the result of the scaled experiment as explained in above Section III.B. The resolution of the image was lowered in Fig. 4 since the $f-$number was increased from 1.286 to 2.143, and the frequency was reduced from 20 MHz to 2.5 MHz. Thus, the size of the digital phantom was increased by a scaling factor of s = 13.33 (see Eq. (13)) (the height between the top-most and the bottom-most point objects was increased from 2.5 mm to 33.33 mm) to make the images in Fig. 4 comparable with the image in Fig. 1(f) that was obtained with the 20-MHz transducer. However, since a larger $f-$number was used in Fig. 4, the image is magnified more relative to the transducer aperture and thus more distortions can be seen around the edges of the images. Also, due to the size of the point source (1 mm in diameter or about 1.7 wavelengths) used in the experiment, the ultrasound field produced was not a perfect spherical wave. This causes additional distortions around the edges of the images. To be comparable with Fig. 1(f), the same number of elements (N = 1004) of the 2D ring array (with an outer diameter of 46.67 mm and an inner diameter of 30 mm) was used in Fig. 4, which gives a pitch of 1.655 λ_2.

As a comparison, a computer simulation [18] using the scaled digital phantom with parameters corresponding to those used in the experiment was performed. The result is shown in Fig. 4(b). It is clear that the simulation data is very close to that of the experiment except near the edges of the image. The better quality of the image around the edges in Fig. 4(b) is due to a smaller point source (about 0.098 mm diameter) that was used and thus a better spherical wave was produced.

Based on a comparison of Figs. 4(a) and 4(b) with Fig. 1(f), it is clear that the quality of images is very similar near the center of the images. The outer edges of the images in Fig. 4 has a lower quality is due to the reasons explained above.

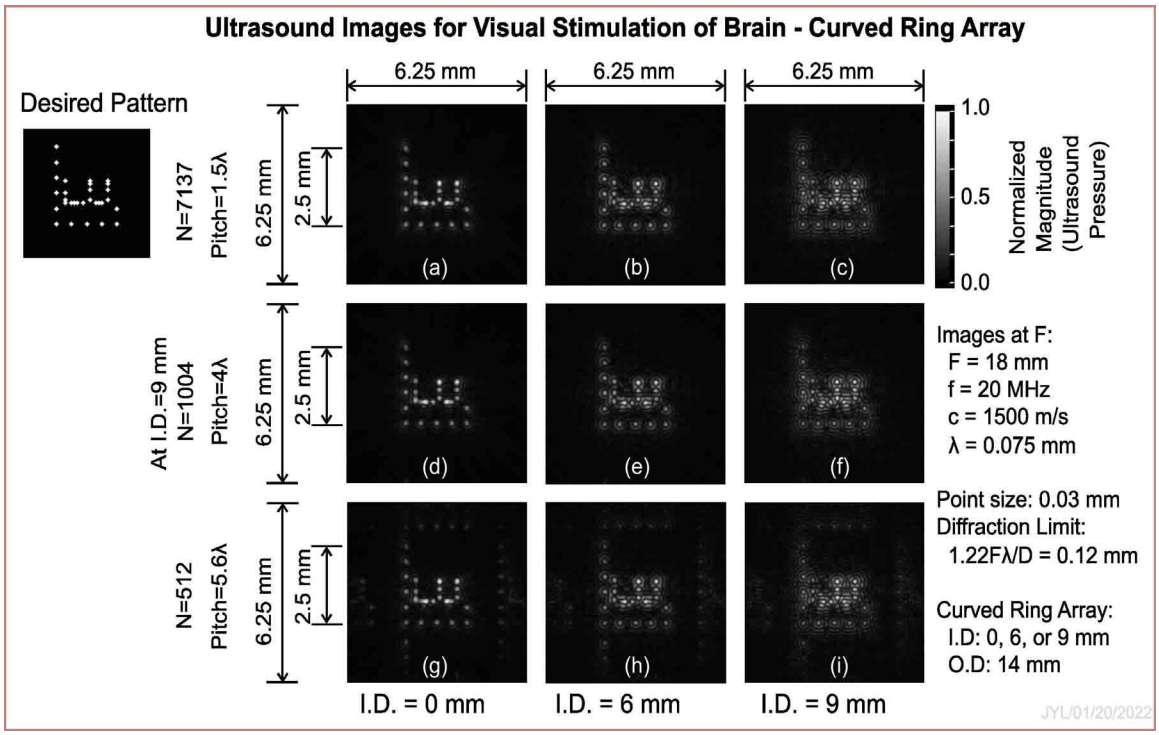

Fig. 1. Ultrasound images of a digital phantom (see the "Desired Pattern" on the upper-left corner) produced at the focal distance with a concave 2D ring array transducer of 20-MHz frequency (0.075-mm wavelengths in water at a speed of sound of about 1500 m/s), 18-mm focal length, 14-mm outer diameter, and a diffraction limit of about 0.12 mm (the radius of the Airy pattern, see Eq. (37) of [27]). The height between the top-most and bottom-most point objects in the digital phantom is 2.5 mm and the size of each point object is about 0.03 mm (smaller than the wavelength of 0.075 mm). There are 30 point objects in the digital phantom. For Panels (a)-(i), from the top to the bottom rows, the pitches of the 2D array are 1.5 (7137 elements when I.D. = 9 mm), 4.0 (1004 elements when I.D. = 9 mm), and 5.6 (512 elements when I.D. = 9 mm) wavelengths respectively. From the left to the right columns, the inner diameters (I.D.) of the ring array are 0, 6, and 9 mm respectively. It is seen from the images in the bottom row that artifacts are produced due to aliasing caused by a large size of the array elements (inadequate spatial sampling rate). The dimensions of each image are shown in the figure, and the grayscale bar represents the normalized magnitude of ultrasound pressure. (Reproduced from [17] with permission.)

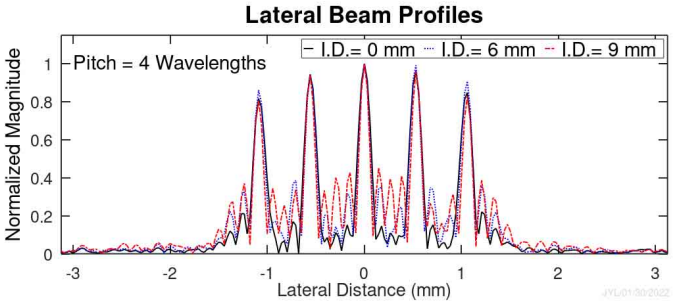

Fig. 2. Line plots through the center of the bottom 5 point objects of the three images obtained with the 20-MHz concave 2D ring array transducer of inner diameters (I.D.) of 0 (solid line), 6 (dotted line), and 9 mm (dashed line) in the middle row (4.0-wavelength pitch) of Fig. 1. The vertical axis represents the normalized magnitude of the ultrasound pressure. It is clear that as the inner diameter is increased, the sidelobes of the point objects in the images also increase. (Modified from [17] with permission.)

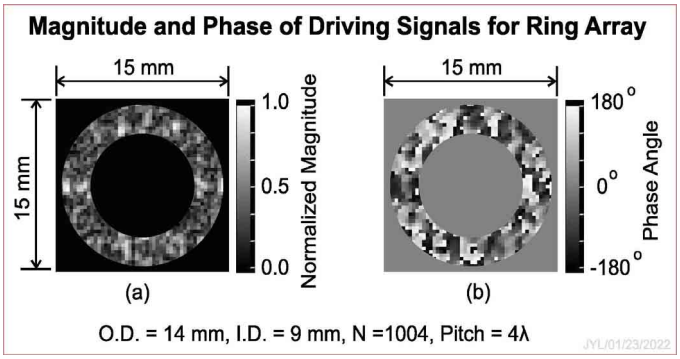

Fig. 3. Magnitude (a) and phase (b) of the electrical drive function for the concave 2D ring array transducer to produce the image in Fig. 1(f). It is seen that because the focusing is handled by the concave shape of the array, a larger size of element (4.0-wavelength pitch) and thus a smaller number of array elements (1004) can be used to produce the image without aliasing artifacts. The blocky looking of the drive function is due to the larger pitch of the array (in the 15 mm x 15 mm images above, there can be a maximum of 47 x 47 = 2209 elements, with 1004 elements between the rings). (Reproduced from [17] with permission.)

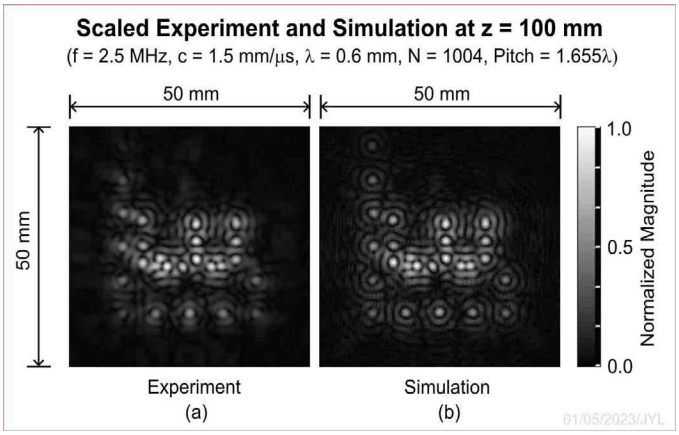

Fig. 4. (a) Ultrasound image experimentally produced with a concave 2D ring array transducer of a lower frequency of 2.5 MHz, 100-mm focal length, 46.67-mm outer diameter, and 30-mm inner diameter using a scaled digital phantom (13.33 times larger than that in Fig. 1). The image produced with a computer simulation using the same parameters as those of the experiment is shown in (b). These images are comparable to that in Fig. 1(f) obtained at a higher frequency and the same number of elements (1004). However, the pitch of the array used here is 1.655 instead of 4.0 wavelengths to maintain the same number of array elements (notice that the wavelength here is 8 times larger than that used in Fig. 1). The dimensions of the images and the grayscale bar are given in the figure.

V. Discussion

The concave 2D ring array transducer studied in this paper can be used to produce images to stimulate multiple points on the retina simultaneously. This is a natural way of stimulation as opposed to the point-by-point method since the optical image of the entire object is formed on the retina to produce vision as people seeing an object. However, since the total power of ultrasound that can be used is limited due to safety reasons, the method spreads the total power over a larger area of the retina and thus the intensity of ultrasound at each point of the retina is lowered. Thus, if the intensity of ultrasound is not adequate for the stimulation, the size of the image may have to be reduced. However, the use of images to stimulate the cells on the retina has the advantage that a dynamic vision can be perceived by the blind people. To achieve this, the images of a moving object can be captured by a small video camera mounted on a frame of a wearable device that is similar to the eyeglasses and then the optical images are Fourier transformed with Eq. (12) to produce electrical drive signals to produce ultrasound images on the retina. The blind people can then "see" the moving object through the visual stimulation of their brain areas.

In terms of image quality, as is seen in Fig. 1, the best ultrasound image is obtained when the inner diameter (I.D.) of the 2D ring array transducer is zero. This is expected since lower sidelobes of point objects can be obtained when the entire 2D array surface is utilized. However, as mentioned before, a large enough inner diameter is needed to avoid the lens area that has a high ultrasound attenuation which can cause heating of the lens material and distort the ultrasound beams. In this study, we chose I.D. = 9 mm for experiments on larger animals such as rabbits.

The concave shape of the 2D ring array transducer is important for two reasons. One is to have a better fit of the array with the geometry of the eyeballs. The second is to focus the ultrasound beam, which removes the need of electronic focusing and thus allows a larger size of the array elements to be used without causing severe aliasing artifacts. From the images in Fig. 1, it is clear that a pitch that is as large as 4.0 λ_1 (a total number of elements of about N = 1004 when I.D. = 9 mm) still produces good images. A smaller number of elements for the 2D ring array transducer will reduce the complexity of the transducer and the number of interconnections, and thus simplify the drive electronics of the imaging system.

Since the Fourier transform relationship in Eq. (12) is based the Fresnel approximation [26], i.e., the size of images cannot be too large in order to satisfy the paraxial condition, larger distortions are expected near the edges of larger images produced.

The images in Fig. 1 were obtained on a flat surface. However, an actual retina is on a curved surface. In this case, the phase term $\exp[-ikr_0^2/(2F)]$ in Eq. (12) can be partially removed (if the curvature of the retina surface is equal to F, the phase term can be completely removed). Also, since the surface of the retina is curved, the distance from the center of the transducer to any points on the retina will be closer to the geometrical focal distance of the transducer and thus the quality of the images near the edges will be better than those obtained in Fig. 1 [27].

It is worth noting that another way of producing images on the retina is to use limited-diffraction beams such as Bessel beams [29] and X wave [30-31] (also see Eqs. (25) and (26) of [27]). Ultrasound image patterns can be designed and the patterns can stay in focus over a large depth of field using the method in [32]. It is also possible that, a zeroth-order Bessel beam (n = 0 in Eq. (25) of [27]) can be shifted and then coherently added to form an arbitrary beam pattern. However, because limited-diffraction beams have larger sidelobes than conventional focused beams at their focuses, the quality of images obtained with the limited-diffraction beams may be lower as compared to the method developed in this paper. Also, the large inner diameter of the 2D ring array and the concave shape of the array will distort the limited-diffraction beams.

VI. Conclusion

A high-frequency (20 MHz) ultrasound concave 2D ring array transducer was designed for the stimulation of retinal cells to subsequently stimulate the corresponding neurons in the visual cortex of the brain for vision perception in blind people. The high-frequency ultrasound produces a high image resolution and allows the transducer to be made small enough to fit the human eyeballs. The ring array has a large enough inner diameter (9 mm) to avoid the lens area where the ultrasound attenuation is high and thus may cause heating of the lens material and distortions of the beam when conducting experiments in large animals such as rabbits. The concave shape of the array will easily fit with the geometrical shape of the eyeball and allows the array to have smaller number of elements but still producing good images without aliasing

artifacts caused by an inadequate spatial sampling rate. The smaller number of elements will reduce the complexity of the array transducer and the number of interconnections, and simplify the driving electronics of the imaging system. Both computer simulations and a scaled experiment were performed, and the results show that good ultrasound images can be produced with this concave 2D ring array transducer for the restoration of vision in blind people.

REFERENCES

[1] L. S. Lim, P. Mitchell, J. M. Seddon, F. G. Holz, and T. Y. Wong. "Age-related macular degeneration." *The Lancet* 379, no. 9827 (2012): 1728-1738.

[2] S. Ferrari, E. D. Iorio, V. Barbaro, D. Ponzin, F. S. Sorrentino, and F. Parmeggiani. "Retinitis pigmentosa: genes and disease mechanisms." *Current genomics* 12, no. 4 (2011): 238-249.

[3] W. H. Dobelle, M. G. Mladejovsky, and J. P. Girvin. "Artificial vision for the blind: electrical stimulation of visual cortex offers hope for a functional prosthesis." *Science* 183, no. 4123 (1974): 440-444.

[4] C. M. Rountree, A. Raghunathan, J. B. Troy, and L. Saggere. "Prototype chemical synapse chip for spatially patterned neurotransmitter stimulation of the retina ex vivo." *Microsystems & Nanoengineering* 3, no. 1 (2017): 1-12.

[5] J. D. Weiland, S. T. Walston, and M. S. Humayun. "Electrical stimulation of the retina to produce artificial vision." *Annu Rev Vis Sci*, 2 (2016): 273-294.

[6] E. Strickland and M. Harris. "What Happens When a Bionic Body Part Becomes Obsolete?: Blind People with Second Sight's Retinal Implants Found Out." *IEEE Spectrum*, 59, no. 3 (2022): 24-31.

[7] A. C. Ho, M. S. Humayun, J. D. Dorn, L. D. Cruz, G. Dagnelie, J. Handa, P.-O. Barale, J.-A. Sahel, P. E. Stanga, F. Hafezi, A. B. Safran, J. Salzmann, A. Santos, D. Birch, R. Spencer, A. V. Cideciyan, E. de Juan, J. L. Duncan, D. Eliott, A. Fawzi, L. C. Olmos de Koo, G. C. Brown, J. A. Haller, C. D. Regillo, L. V. Del Priore, A. Arditi, D. R. Geruschat, R. J. Greenberg, "Long-term results from an epiretinal prosthesis to restore sight to the blind." *Ophthalmology* 122, no. 8 (2015): 1547-1554.

[8] O. Naor, Y. Hertzberg, E. Zemel, E. Kimmel, and S. Shoham. "Towards multifocal ultrasonic neural stimulation II: design considerations for an acoustic retinal prosthesis." *Journal of neural engineering* 9, no. 2 (2012): 026006.

[9] M. D. Menz, O. Oralkan, P. T. Khuri-Yakub, and S. A. Baccus. "Precise neural stimulation in the retina using focused ultrasound." *Journal of Neuroscience*, 33, no. 10 (2013): 4550-4560.

[10] X. Wu, M. Kumar, and O. Oralkan. "An ultrasound-based noninvasive neural interface to the retina." In *2014 IEEE International Ultrasonics Symposium*, pp. 2623-2626. IEEE, 2014.

[11] M. Gao, Y. Yu, H. Zhao, G. Li, H. Jiang, C. Wang, F. Cai, L. L.-H. Chan, B. Chiu, W. Qian, W. Qiu, and H. Zheng. "Simulation study of an ultrasound retinal prosthesis with a novel contact-lens array for noninvasive retinal stimulation." *IEEE Transactions on Neural Systems and Rehabilitation Engineering*, 25, no. 9 (2017): 1605-1611.

[12] G. Lu, X. Qian, R. Li, B. Thomas, M. S. Humayun, and Q. Zhou, "Non-invasive ultrasound stimulation on the retina and visual cortex for visual restoration," *Journal of Acoustical Society of America*, vol. 150, no. 4, pt. 2, pp. A207, 2021.

[13] X. Qian, G. Lu, B. B. Thomas, R. Li, X. Chen, K. K. Shung, M. Humayun, and Q. Zhou. "Noninvasive Ultrasound Retinal Stimulation for Vision Restoration at High Spatiotemporal Resolution." *BME Frontiers*, 2022 (2022).

[14] L. Jiang, G. Lu, Y. Zeng, Y. Sun, H. Kang, J. Burford, C. Gong, M. S. Humayun, Y. Chen, and Q. Zhou. "Flexible ultrasound-induced retinal stimulating piezo-arrays for biomimetic visual prostheses." *Nature communications*, 13, no. 1 (2022): 1-13.

[15] Yoni Hertzberg, Omer Naor, Alexander Volovick, and Shy Shoham. "Towards multifocal ultrasonic neural stimulation: pattern generation algorithms." *Journal of neural engineering*, 7, no. 5 (2010): 056002.

[16] Dong-Lai Liu, and Robert C. Waag. "Propagation and backpropagation for ultrasonic wavefront design." *IEEE transactions on ultrasonics, ferroelectrics, and frequency control*, 44, no. 1 (1997): 1-13.

[17] Jian-yu Lu, Gengxi Lu, Mark Humayun, and Qifa Zhou. "Concave 2D Ring Array Transducer for Ultrasound Visual Stimulation of the Brain." In *2022 IEEE International Ultrasonics Symposium (IUS)*, pp. 1-4. IEEE, 2022.

[18] Jian-yu Lu and Jiqi Cheng, "Field computation for two-dimensional array transducers with limited diffraction array beams," *Ultrasonic Imaging*, vol. 27, no. 4, pp. 237-255, October 2005.

[19] F. John, *Partial Differential Equations*. New York: Springer-Verlag, 1982.

[20] Jian-yu Lu, "Limited diffraction array beams," *International Journal of Imaging System and Technology*, vol. 8, no. 1, pp. 126-136, January 1997.

[21] Jian-yu Lu, "2D and 3D high frame rate imaging with limited diffraction beams," *IEEE Transactions on Ultrasonics, Ferroelectrics, and Frequency Control*, vol. 44, no. 4, pp. 839-856, July, 1997.

[22] Jian-yu Lu, Jiqi Cheng, and Jing Wang, "High frame rate imaging system for limited diffraction array beam imaging with square-wave aperture weightings," *IEEE Transactions on Ultrasonics, Ferroelectrics, and Frequency Control*, vol. 53, no. 10, pp. 1796-1812, October 2006.

[23] Jiqi Cheng and Jian-yu Lu, "Extended high frame rate imaging method with limited diffraction beams," *IEEE Transactions on Ultrasonics, Ferroelectrics, and Frequency Control*, vol. 53, no. 5, pp. 880-899, May 2006.

[24] R Bracewell, *The Fourier transform and its applcmions*. New York: McGraw-Hill. 1965.

[25] E. O. Brigham, *The fast Fourier transform.* Englewood Cliffs, NJ: Prentice-Hall, 1974.

[26] J. W. Goodman, *Introduction to Fourier Optics*. New York McGraw-Hill., 1968.

[27] Jian-yu Lu, "Focused beams for high-resolution imaging and other applications," in *Proceedings of Meetings on Acoustics* (POMA), pp.1-13, vol. 45, no. 1, 020001 (2021), March 21, 2022 (Acoustical Society of America, DOI: 10.1121/2.0001544).

[28] Lu, Jian-yu. "Producing bowtie limited diffraction beams with synthetic array experiment." *IEEE Transactions on Ultrasonics, Ferroelectrics, and Frequency Control* 43, no. 5 (1996): 893-900.

[29] Jian-yu Lu and James F. Greenleaf. "Ultrasonic nondiffracting transducer for medical imaging." *IEEE transactions on ultrasonics, ferroelectrics, and frequency control* 37, no. 5 (1990): 438-447.

[30] Jian-yu Lu and J. F. Greenleaf, "Nondiffracting X waves --- exact solutions to free-space scalar wave equation and their finite aperture realizations," *IEEE Transactions on Ultrasonics, Ferroelectrics, and Frequency Control*, vol. 39, no. 1, pp. 19-31, January 1992.

[31] Jian-yu Lu and J. F. Greenleaf, "Experimental verification of nondiffracting X waves," *IEEE Transactions on Ultrasonics, Ferroelectrics, and Frequency Contro*l, vol. 39, no. 3, pp. 441-446, May 1992.

[32] Jian-yu Lu, "Designing limited diffraction beams," *IEEE Transactions on Ultrasonics, Ferroelectrics, and Frequency Control*, vol. 44, no. 1, pp. 181-193, January 1997.

Jian-yu Lu (S'86--M'88--SM'99--F'08) received the B.S. degree in physics/electrical engineering in February 1982 from Fudan University, Shanghai, China; the M.S. degree in physics/acoustics in 1985 from Tongji University, Shanghai, China; and the Ph.D. degree in biomedical engineering in 1988 from Southeast University, Nanjing, China. From December 1988 to February 1990, he was a Postdoctoral Research Fellow at Mayo Medical School, Rochester, Minnesota, USA.

Since 1997, Dr. Lu has been a professor in the Department of Bioengineering at The University of Toledo (UT), Toledo, OH, USA,

and since 1998, he has been an adjunct professor in the College of Medicine and Life Sciences. Before joining UT as a professor in 1997, he was an associate professor of biophysics at Mayo Medical School and an Associate Consultant at the Department of Physiology and Biophysics, Mayo Clinic/Foundation, Rochester, MN, USA. His research interests are in acoustic imaging and tissue identification, medical ultrasonic transducers, and ultrasonic beam forming and propagation.

Dr. Lu received the Outstanding Paper Award from the IEEE UFFC Society (UFFC-S) for two of his papers published in the IEEE TUFFC in 1992 for the discovery of X wave. In addition, he received the Edward C. Kendall Award for his meritorious research from the Mayo Alumni Association in 1992, the NIH FIRST Award in 1991, Distinguished Service Award from UFFC-S in 2016, and the Engineer of the Year Award from the IEEE Toledo Section in 2021.

Dr. Lu served as the President of IEEE UFFC-S from 2014-2015, the Editor-in-Chief of IEEE TUFFC from 2002-2007, the General Chair of 2008 IEEE IUS, the Technical Program Committee (TPC) Chair of 2001 IEEE IUS, a member of the Editorial Board of IEEE Access from 2016-2021, an Elected AdCom member of IEEE UFFC Society from 2009-2011, and many committees of UFFC-S. In addition, he served in IEEE Toledo Section.

Dr. Lu is a Fellow of IEEE (conferred in 2008), a Fellow of the American Institute of Ultrasound in Medicine (AIUM) (conferred in 2005), and a Fellow of the American Institute for Medical and Biological Engineering (AIMBE) (conferred in 2007).

Gengxi Lu received his Ph.D. degree with the Department of Biomedical Engineering, University of Southern California, Los Angeles, CA, USA in 2022. And the bachelor's degree in physics from Nanjing University, Nanjing, China, in 2017. His research interests include the ultrasound neuromodulation, ultrasound functional imaging, 3-D printing, and the development of advanced ultrasound devices.

Biju Thomas received his PhD in behavioral neuroscience from the Department of Zoology, University of Kerala, India in 1997. In January 2001, he joined the retinal transplant program at the Department of Ophthalmology, University of Louisville, KY as a Postdoctoral fellow to perform behavioral and electrophysiological evaluation of visual function in rodents. In 2002 he moved to the newly founded USC Retina Institute and continued his post-doctoral studies on visual functional evaluations in rodents. As an Associate Professor of Research in Ophthalmology at University of Southern California (USC) Vision Science Institute, Dr. Thomas is currently leading a laboratory focused on developing new therapies for retinal degeneration diseases. He has published more than 40 peer reviewed research papers with majority pertaining to therapies for retinal diseases.

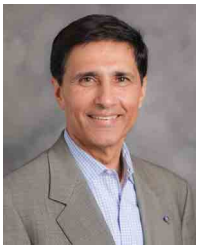

Mark S. Humayun, MD, PHD, is the Cornelius J. Pings Chair in Biomedical Sciences, Professor of Ophthalmology, Biomedical Engineering, and Integrative Anatomical Sciences, Director of the USC Ginsburg Institute for Biomedical Therapeutics, and Co-Director of the USC Roski Eye Institute.

Dr. Humayun is an internationally recognized pioneer in vision restoration. He assembled a team of multidisciplinary experts to develop the first FDA approved artificial retina, Argus II, for sight restoration. He has more than 140 issued patents and over 300 peer reviewed publications. He has a google scholar H index of 102.

Dr. Humayun is a member of the U.S. National Academies of Medicine, Engineering, and Inventors. He is a Fellow of the American Association for the Advancement of Science (AAAS), Institute of Electrical and Electronics Engineers (IEEE), American Society of Retinal Specialists (ASRS), and Association for Research in Vision and Ophthalmology (ARVO).

For his extraordinary contributions he was awarded the United States' highest technological achievement, the 2015 National Medal of Technology and Innovation by President Obama. He is the recipient of the 2018 IEEE Biomedical Engineering Award, the 2020 IEEE Medal for Innovations in Healthcare Technology, and the Charles Schepens award by the American Academy of Ophthalmology in 2021. Dr. Humayun was named top 1% of ophthalmologists by the U.S. News & World Report.

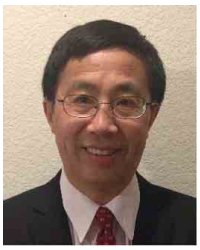

Qifa Zhou (F'19) received the Ph.D. degree from the Department of Electronic Materials and Engineering, Xi'an Jiaotong University, Xi'an, China, in 1993. Before joining the University of Southern California (USC), Los Angeles, CA, USA, in 2002, he worked with the Department of Physics, Sun Yat-sen University, Guangzhou, China; the Department of Applied Physics, The Hong Kong Polytechnic University, Hong Kong; and the Materials Research Laboratory, Pennsylvania State University, State College, PA, USA. He is currently a Professor of biomedical engineering and ophthalmology with USC. He has authored or coauthored more than 200 peer-reviewed articles in journals including Nature Medicine, Advanced Materials, and Progress in Materials Science. His research focuses on the development of piezoelectric high-frequency ultrasonic transducers for biomedical ultrasound and photoacoustic imaging, including intravascular imaging, cancer imaging, and ophthalmic imaging. He is also actively exploring ultrasonic mediated therapeutic technology including trans-sclera drug delivery, as well as ultrasound for retinal and brain stimulation.

Dr. Zhou is a fellow of the International Society for Optics and Photonics (SPIE) and the American Institute for Medical and Biological Engineering (AIMBE) and a member of the Technical Program Committee of the IEEE International Ultrasonics Symposium. He is an Associate Editor of the IEEE Transactions on Ultrasonics, Ferroelectrics, and Frequency Control.